Numerical Study of a Ramjet Dump Combustor Flowfield

J. Philip Drummond*
NASA Langley Research Center, Hampton, Virginia

Increased interest in ramjet propulsion systems with higher performance requirements and tighter constraints on system size and weight has lead to the need for improved techniques for analyzing and designing such systems. A computer program has been developed to analyze the turbulent reacting flowfield in a ramjet dump combustor configuration. The program solves the axisymmetric Navier-Stokes and species equations throughout the engine diffuser and combustor providing a unified analysis of the engine flowfield, including flow separation, fuel-air mixing, and initial results with chemical reaction. Details of the program development are given, along with a comparison of program results with data from a dump combustor simulation experiment, to allow assessment of the flowfield modeling that is employed.

Nomenclature

A,B = thermodynamic coefficients
c = specific heat at constant pressure
D = outer pipe diameter
f = hydrogen mass fraction
H = total enthalpy
L = finite difference operator
ℓ = mixing length
M = Mach number
p = pressure
R = outer pipe radius
T = temperature
t = time
U_i = initial velocity of primary air jet
u,v = streamwise and transverse velocity components
w = weighting function in coordinate transformation
x,r = streamwise and transverse physical coordinates
α = species mass fraction
β_x,β_r = coordinate stretching parameters
γ = ratio of specific heats
δ = boundary-layer thickness
η,ξ = transverse and streamwise computational coordinates
$\bar{\eta},\bar{\xi}$ = transverse and streamwise nondimensional physical coordinates
μ = viscosity
ρ = density

Superscripts

n = time index
0 = reference value at standard conditions

Subscripts

c = chemical potential
i,j = grid indices
k = chemical species index
P = chemical products
R = chemical reactants
r = transverse direction
T = total conditions
t = turbulent
x = streamwise direction

Presented as Paper 83-0421 at the AIAA 21st Aerospace Sciences Meeting, Reno, Nev., Jan. 10-13, 1983; received Oct. 21, 1983; revision received March 29, 1984. This paper is declared a work of the U.S. Government and therefore is in the public domain.

*Aerospace Engineer, Computational Methods Branch, High-Speed Aerodynamics Division.

Introduction

INCREASED interest in ramjet propulsion systems (see Fig. 1) with higher performance requirements and tighter constraints on system size and weight has led to the need for improved techniques for analyzing and designing such systems. A critical requirement for achieving high system performance within specified geometric limits is an accurate description of the combustor flowfield, including the effects of turbulence and chemical reaction. Unfortunately, the flowfield phenomena present in a ramjet combustor are quite complex, and direct solution of the governing equation system, including the full Navier-Stokes equations, chemical kinetics equations, and appropriate modeling of the turbulence field, is not yet a realistic option. Although limited analyses using the governing equations (i.e., a unified approach) have been attempted, the difficulties mentioned above typically have led to the development of modular modeling techniques, where various regions of the ramjet combustor are modeled separately, and the results are then coupled to provide a complete flowfield description.

Calculations of a dump combustor flowfield with massive separation requires the solution of the spatially elliptic form of the governing equations in that axial diffusion is an important process within the separation. Therefore, the equation system cannot be simplified in this region by parabolization. Successful solutions for recirculating flow with reaction have been described in the literature, for instance, the work by Hutchinson et al.[1] and Abou Ellail et al.[2] Both report, however, the need to carefully adapt the modeling employed in their analysis to the particular experimental case being analyzed to achieve their successful comparisons.[3] The need for careful modeling is not surprising though, since a detailed understanding of the complex phenomena involved in these flowfields still remains beyond the state-of-the-art.

It is for this reason that modular models have evolved for the prediction of ramjet flowfields. These models draw upon an experimental knowledge of the flowfield that is then used to divide the flow into several appropriate regions or zones. Each of the zones can then be mathematically decoupled, analyzed individually, and then recoupled through some appropriate model to provide an overall description of the flowfield. A number of examples of the modular approach are available in the literature, for instance, Edelman et al.,[3] Harsha et al.,[4] Viets and Drewry,[5] and Swithenbank et al.[6] Typically, these models represent the flow separation behind the step with a well stirred reactor model[4] and the central core of the flow with the parabolic form of the governing equations. These two regions are then coupled together with a shear layer model to complete the description of the flowfield. The modular models obviously require a number of assump-

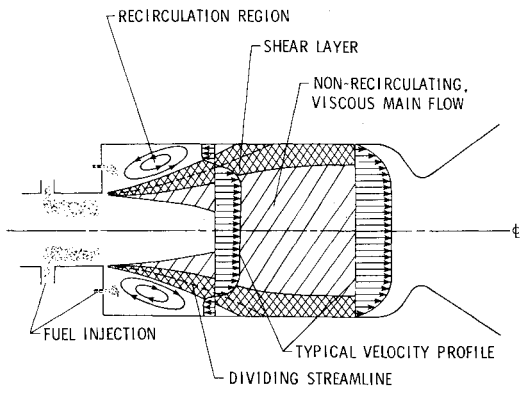

Fig. 1 Schematic of ramjet dump combustor flowfield.[3]

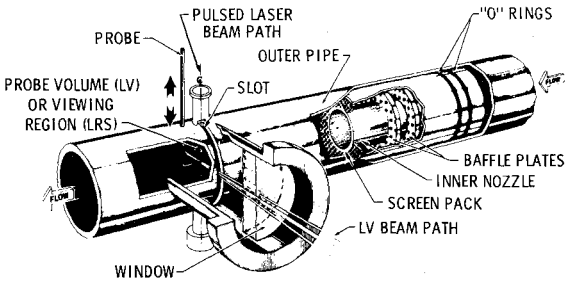

Fig. 2 Dump combustor simulation facility.[7]

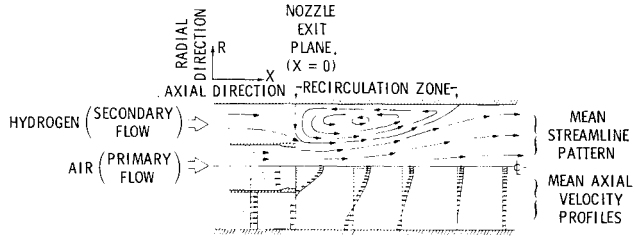

Fig. 3 Typical flowfield in dump combustor simulation facility.[7]

tions regarding the structure of the flowfield. However, the models do perform well when developed for a particular configuration and applied parametrically over a range about the initial design configuration.

The intent of the present work is to develop a computational procedure for calculating important parameters in a ramjet dump combustor using the "unified" approach; i.e., computing the entire flowfield as a unit rather than in parts and patching the results together. The flowfield is described using the spatially elliptic form of the governing equation system. Modeling of the turbulence field and chemical reaction is done using fairly straightforward models, without attempting to optimize them to the flowfields being considered. The computational procedure that results from this approach is then applied to a ramjet dump combustor simulator for which detailed experimental data are available. The computed results and data are then compared for both nonreacting and reacting flows of gaseous hydrogen fuel and air to allow assessment of the overall modeling procedure that is employed. Conclusions are finally drawn regarding modeling improvements that are needed to improve the comparison. The present work should then provide a point of departure for modeling improvements planned in the future.

Experiment

A ramjet dump combustor simulation experiment was carried out at the Arnold Engineering Development Center. Data collected from that experiment are compared with results of the analysis technique discussed in this paper. Details of the experiment and a tabulation of the data are given in Ref. 7. A brief discussion of the experiment is given here for completeness.

A ramjet dump combustor flowfield was simulated by this experiment using the configuration shown in Fig. 2. Air was injected from the inner 5.25-cm pipe at a mass-flow rate of 0.263 kg/s, a total temperature and pressure of 289 K and 100,748 Pa, respectively, and a bulk velocity of 102 m/s. The inner air nozzle was surrounded by a 13.31-cm outer pipe from which gaseous hydrogen was injected at a mass-flow rate of 0.001 kg/s, a total temperature and pressure of 311 K and 93,191 Pa, respectively, and a bulk velocity of 0.92 m/s. The diameter ratio of this configuration was 2.5. The hydrogen gas was passed through two porous plates and a screen pack to stabilize the flow before being introduced into the duct downstream of the primary air nozzle. This assembly resulted in a barrier with the appearance of a rearward-facing step to the primary airflow.

A viewing port or slot was provided downstream of the gas injection location to provide optical access for laser velocimetry instrumentation for measurement of pertinent flowfield data. A pitot and gas sampling probe was also sited near this location. The nozzle assembly could be moved axially relative to the data collection station to allow measurement between zero and six outer pipe diameters downstream. Data collected by the system included radial distribution of total pressure, mean axial and radial velocity, turbulence intensity, total hydrogen mass fraction, velocity cross correlation, static temperature, and wall static pressure distributions.

The typical flowfield in the dump combustor simulator is shown in Fig. 3. The flow contains the basic features known to exist in ramjet engines including a primary streamwise flow, a separated recirculating flow behind the hydrogen injection station (step simulator), and a shear layer connecting these two regions which grows radially with increasing axial distance. The work described in the following sections of this paper concerns the numerical modeling of this flowfield. The analysis employed to accomplish this modeling is discussed in the following section.

Analysis

Governing Equations

The flowfield in a ramjet dump combustor can be described by the spatially elliptic and temporally parabolic form of the compressible Navier-Stokes equations and one or more additional transport equations describing the species present in the flow. These equations written in conservation law form for a two-component gas in an axisymmetric configuration are given by

$$\frac{\partial U}{\partial t}+\frac{\partial F}{\partial x}+\frac{1}{r}\frac{\partial (rG)}{\partial r}+\frac{H}{r}=0 \tag{1}$$

Elements of the vectors U, F, G, and H are described in Ref. 8. The compressible form of the governing equations is retained to account for local compressibility effects associated with reaction and allow for the option of coupling a supersonic inlet and/or nozzle into the present analysis. The flowfield is modeled by assuming that it behaves as a real gas with thermodynamic quantities being functions of local temperature and species concentrations.[8] The pressure is calculated from the equation of state using a mixture gas constant, and the laminar viscosity is estimated from Sutherland's law. The turbulent viscosity is estimated from an algebraic eddy-viscosity model to be described later in the paper.

Coordinate Transformation

In order to resolve large flowfield gradients, the physical coordinate grid must be fine near walls and through major disturbances in the flowfield, including flow near the step and within the separation and shear layer downstream of the step. Well away from these regions, a coarser physical grid can be used for computational efficiency while still adequately resolving the flowfield. Therefore, a transformation of the independent variables is needed to transform the resulting nonuniform grid in the physical domain to a uniform grid in the computational domain.

The algebraic-numerical coordinate transformation of Smith and Weigel[9] is used to transform the governing equation (1). This work is thoroughly discussed in the literature and, therefore, will not be repeated here. However, the function chosen to compress the grid near the engine walls and within the separation and shear layer applied by means of this transformation will be discussed.

The compression function of Roberts[10] is used to compress the grid near longitudinal walls. Its inverse is given by

$$\bar{\eta}_1 = \left[(\beta_r+2\alpha)\left(\frac{\beta_r+1}{\beta_r-1}\right)^{(\eta-\alpha)/(1-\alpha)} - \beta_y + 2\alpha\right] \div \left\{(2\alpha+1)\left[1+\left(\frac{\beta_r+1}{\beta_r-1}\right)^{(\eta-\alpha)/(1-\alpha)}\right]\right\} \tag{2}$$

where $\bar{\eta}_1 = r/R$. For $\alpha = 0.5$, the grid is transversely compressed near the centerline ($r=0$) and the longitudinal wall ($r=R$). For $\alpha = 0$, the grid is compressed only at the longitudinal wall.

The compression function of Thomas et al.[11] is used to compress the grid transversely through the shear layer downstream of the step. Its inverse is given by

$$\bar{\eta}_2 = \eta_0\left[\frac{\sinh(\beta_{yi}\eta - A_\eta)}{\sinh A_\eta} + 1\right] \tag{3}$$

where

$$A_\eta = \frac{1}{2}\ell n\left[\frac{1+(e^{\beta_{ri}}-1)\eta_0}{1+(e^{-\beta_{ri}}-1)\eta_0}\right]$$

and η_0 is the value of η at which maximum compression occurs. In order for this function to track the development of the shear layer downstream of the step, it should allow the grid to expand as the shear layer develops. To allow this freedom, β_{ri} is chosen to be a linear function of ξ, such that

$$\beta_{ri} = \beta_{ri_{\min}} + (\beta_{ri_{\max}} - \beta_{ri_{\min}})(1-\xi) \tag{4}$$

where $\beta_{ri_{\min}}$ and $\beta_{ri_{\max}}$ are the minimum and maximum values, respectively, of the β_{ri} compression coefficient.

Equations (2) and (3) are combined to form the overall transverse compression $\bar{\eta}$, using a weighting function w, to give

$$\bar{\eta} = \bar{\eta}_1 w + \bar{\eta}_2(1-w) \tag{5}$$

where

$$w = 1 + (w_{\min}-1)\frac{\eta}{\eta_0} \qquad 0 \le \eta \le \eta_0$$

$$= w_{\min} + (1-w_{\min})\frac{\eta-\eta_0}{1-\eta_0} \qquad \eta_0 < \eta \le 1$$

and $w_{\min}$ is the minimum allowable value of the weighting function w. In Eq. (5), the weighting causes the $\bar{\eta}_2$ compression to predominate near η_0 and the $\bar{\eta}_1$ compression to predominate elsewhere.

The function $\bar{\xi}$ defines the longitudinal compression near the step. The compression function of Thomas et al.[11] is used again, but, in this case, along the ξ direction giving

$$\bar{\xi} = \xi_0\left[\frac{\sinh(\beta_x\xi - A_\xi)}{\sinh A_\xi} + 1\right] \tag{6}$$

where

$$A_\xi = \frac{1}{2}\ell n\left[\frac{1+(e^{\beta_x}-1)\xi_0}{1+(e^{-\beta_x}-1)\xi_0}\right]$$

and ξ_0 is the value of ξ at which maximum compression occurs.

Specifying a dependence of β_{ri} on ξ results in $\bar{\eta}$ being a function of both ξ and η, rather than simply η as in Ref. 9. The relationship between points in the physical and computational domains, therefore, must reflect this generalization. The relationship between these points now becomes

$$x = X_2(\bar{\xi})\bar{\eta}(\xi,\eta) + X_1(\bar{\xi})[1-\bar{\eta}(\xi,\eta)]$$

$$y = Y_2(\bar{\xi})\bar{\eta}(\xi,\eta) + Y_1(\bar{\xi})[1-\bar{\eta}(\xi,\eta)] \tag{7}$$

where (X_1, Y_1) are boundary points at $r=0$ and (X_2, Y_2) are boundary points at $r=R$. Elements of the inverse Jacobian matrix are then rederived from Eqs. (7) to complete the modifications to the transformation of Ref. 9.

Turbulence Model

The turbulence field in this study is calculated using the algebraic eddy-viscosity model described in Ref. 12. This mixing-length model is modified to account for turning of the flow near the step by replacing the transverse derivative of the streamwise velocity, $\partial u/\partial r$, by the total rate of strain of the flowfield ζ, where

$$\zeta = \frac{\partial u}{\partial r} + \frac{\partial v}{\partial x}$$

The local turbulent viscosity is then given by

$$\mu_t = \rho\ell^2|\zeta| \tag{8}$$

and the mixing length ℓ is defined by

$$\ell = C_k r D \qquad 0 \le r \le \lambda\delta/C_k$$

$$= \lambda\delta D \qquad r > \lambda\delta/C_k \tag{9}$$

In Eqs. (9), C_k and λ are constants and D is the van Driest damping coefficient as defined in Ref. 12. Values suggested in the reference for C_k and λ are 0.435 and 0.09.

A relaxation model also is employed with the turbulence model to account for memory of the turbulence field. The turbulence field does not respond immediately to rapid changes in the geometry and mean flow downstream of the step, but rather should retain some memory of the turbulence field upstream of the step. The relaxation model of Shang and Hankey[13] is used in this work to model the relaxed eddy viscosity. Along each streamline, downstream of the step, the turbulent viscosity is given by[14]

$$\mu_t = \mu_{t_{\text{step}}} + (\mu_{t_{\text{local}}} - \mu_{t_{\text{step}}})\{1-\exp[-(x-x_{\text{step}})/10\delta]\} \tag{10}$$

where δ is the local boundary-layer thickness at the step.

The turbulent Prandtl number is assumed to be 0.7 in this work, as suggested by Ref. 13 for round jet-like flows. The

turbulent Schmidt number is also set equal to 0.7 following an assumption of unity for the Lewis number.

Solution of the Governing Equations

The unsplit finite difference technique of MacCormack[15] is used to integrate the governing equations until a steady-state solution is reached. If a solution to Eqs. (1) is known at some time step $t=n\Delta t$, then the solution at the next time step $t=(n+1)\Delta t$ can be calculated from

$$U_{i,j}^{n+1}=L(\Delta t)U_{i,j}^{n} \tag{11}$$

for each node point in a finite difference grid network within the boundaries of the computational domain. Details of the finite difference operator L have been discussed numerous times in the literature, therefore, that discussion will not be repeated here. The reader is referred to Ref. 15 for details. Artificial viscosity, other than that inherent in the MacCormack technique itself, is not needed due to the lack of very strong flowfield gradients, typically present in supersonic flows, but not present in the current subsonic analysis.

Boundary and Initial Conditions

No-slip ($u=0$, $v=0$) boundary conditions were used along the pipe walls to specify the velocity components. The wall was assumed adiabatic requiring the normal derivative of temperature to vanish. The normal derivative of the total hydrogen mass fraction was also required to vanish at the walls to satisfy the adiabatic wall assumption for nonreacting flows and the additional assumption of a noncatalytic wall for reacting flows. The wall pressure was calculated from the boundary-layer assumption that its normal derivative vanished at the wall, and density was calculated from the equation of state. Symmetry conditions were applied for all flowfield variables at the pipe centerline.

For subsonic flow, characteristic theory allows three quantities to be specified at the inflow boundaries. At the air inflow boundary, the total pressure, total temperature, and flow angle are specified and their values held constant. Experimentally, this behavior has also been observed. Well upstream of the hydrogen inflow boundary the streamwise static pressure gradient is observed to essentially vanish, and this behavior is also employed in the analysis to define the static pressure at the inflow boundary; i.e., $p_{1,j}=p_{2,j}$. Knowing at the inflow boundary the total pressure, static pressure, and total temperature, the static temperature can be calculated from the isentropic relation

$$\frac{T_T}{T}=\left(\frac{p_T}{p}\right)^{(\gamma-1)/\gamma} \tag{12}$$

which then defines the speed of sound. Further, the Mach number can be calculated from

$$M=\sqrt{2\left[\frac{(T_T/T)-1}{(\gamma-1)}\right]} \tag{13}$$

allowing calculation of the streamwise component of velocity. Knowing the flow angle, the transverse component of velocity can then be calculated. The density and total internal energy can then be computed to complete the specification of conditions at the air inflow boundary.

The Mach number is quite low ($M<0.01$) at the hydrogen inflow boundary. Therefore, three static conditions, the streamwise and transverse components of velocity, and static temperature, are specified there. The streamwise pressure gradient should be small, and the pressure is calculated by assuming that this gradient vanishes. The density and total internal energy can then be computed to complete specification at the hydrogen inflow boundary.

At the subsonic outflow boundary, characteristics theory allows the specification of only one quantity, and only the outflow static pressure is specified. The remaining flowfield quantities are computed using first-order extrapolation from upstream values.

Initial conditions are specified by computing the air inflow conditions using the procedure described above and using these values at all points between the centerline and the inner pipe radius. Between the inner and outer pipe radii, all conditions are set equal to air conditions other than the velocity components, which are set to zero. Although conditions closer to steady state could have been estimated and used to initialize the calculation, such a procedure was not used to avoid prejudicing the final computed results.

Chemistry Model

The chemical reaction of hydrogen fuel and air is modeled in the present work using a complete reaction model. This model assumes that instantaneous reaction occurs at any point where both fuel and air are present. The extent of reaction is determined by the stoichiometric limit of the hydrogen-air reaction; i.e., the amount of hydrogen present determines the extent of reaction with a fuel-lean condition, and the amount of oxygen present determines the extent of reaction with a fuel-rich condition. No reaction is allowed when the fraction of hydrogen in air is less than 4% by volume.

Once the new composition is determined at a given computational node after reaction, the total enthalpy of the products, which must equal the total enthalpy of the reactants, is given by

$$H_p=\sum_k\int_{T^0}^{T}\alpha_k c_k\,dT+\frac{u^2+v^2}{2}+H_c \tag{14}$$

where

$$H_c=[\alpha_{H_2}H_{H_2}^0+\alpha_{H_2O}H_{H_2O}^0+\alpha_{N_2}H_{N_2}^0+\alpha_{O_2}H_{O_2}^0]_{T=T^0}$$

Over the range of temperatures being considered in this work, it is reasonable to assume that the specific heat for each species is a linear function of temperature; i.e.,

$$c_k=A_kT+B_k \tag{15}$$

Substituting Eq. (15) into Eq. (14) and integrating gives

$$H_R=\tfrac{1}{2}\bar{A}_pT^2+\bar{B}_pT-\bar{h}_p^0+[(u^2+v^2)/2]+(H_c)_{T^0}$$

where

$$\bar{h}_p^0=\tfrac{1}{2}\bar{A}_pT^{0^2}+\bar{B}_pT^0$$

$$\bar{A}_p=\sum_k\alpha_kA_k,\qquad \bar{B}_p=\sum_k\alpha_kB_k$$

Solving for T and selecting only the positive root yields the temperature after reaction

$$T=(-\bar{B}_p+\sqrt{\bar{B}_p^2+2\bar{A}_pH_T})/\bar{A}_p \tag{16}$$

where

$$H_T=H_R+\bar{h}_p^0-[(u^2+v^2)/2]-(H_c)_{T^0}$$

The chemistry model is applied at the end of every 200 computational time steps. Once the new composition (hydrogen, oxygen, nitrogen, and water) is known, a new temperature is determined at each computational node, and the gas mixture properties and heat fluxes are recomputed. The calculation then proceeds through the next 200 time steps.

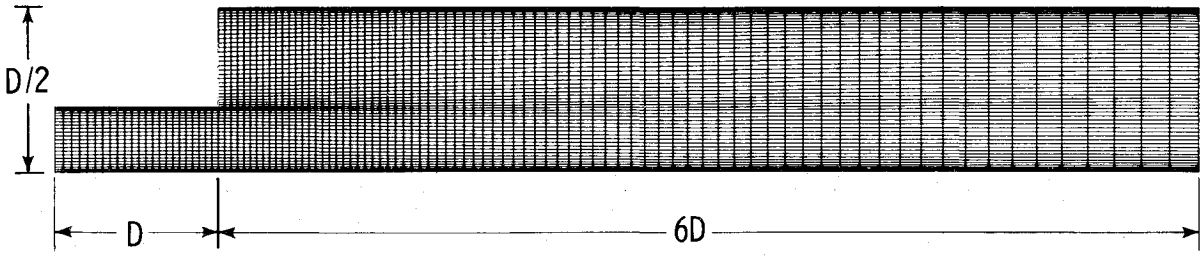

Fig. 4 Finite difference grid used to compute dump combustor flowfield.

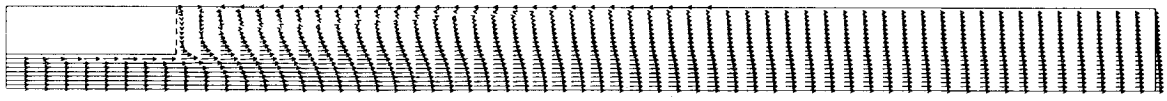

Fig. 5 Computed steady-state velocity vector field in dump combustor simulator.

Results

Using the techniques developed in the preceding section, the flowfield in the ramjet dump combustor simulator was computed. Comparisons of the analytical results and experimental data are given in this section to allow assessment of the modeling that is employed. After discussing these comparisons, conclusions are drawn regarding the validity of the modeling and changes in modeling that are needed to improve the analytical approach.

The analysis of the dump combustor flowfield was carried out in a physical domain beginning one outer pipe diameter (hereafter referred to as diameter) upstream of the step and concluding 6 diameters downstream of the step. Experimental data were collected only downstream of the step, but the computational region upstream of the step was required to maintain a stable solution at the step and allow appropriate specification of boundary conditions. The finite difference grid used to compute the flowfield is given in Fig. 4. The grid has 101 points in the streamwise direction and 51 points in the transverse direction. Note that the grid is compressed transversely near the pipe wall, the step, and the pipe centerline, and it is compressed longitudinally near the step. Note also that the transverse compression near the step expands with the shear layer with downstream movement away from the step. The computations discussed below were also carried out on several coarser grids, without a significant change in the final results.

The resulting nonreacting steady-state velocity field computed on the 101×51 grid for the dump combustor simulator is given in Fig. 5. Steady state is defined as being reached when a relative change in streamwise velocity, $\Delta u/u$, of 10^{-6} is achieved locally at each computational node. The qualitative flowfield features indicated in Fig. 3 have been predicted by the program. Note the massive separation that forms downstream of the step, thinning with distance downstream of the step, and finally reattaching about 3 diameters downstream. Due to relatively low momentum associated with the hydrogen injection, the separation persists upstream to the step face. Note also the shear layer that forms at the lip of the step, creating a mixing region for the hydrogen fuel and primary air. The shear layer thickens downstream of the step and spreads across the entire duct by the end of the pipe.

Quantitative comparisons of the computational and experimental data for nonreacting flow are given in Figs. 6-10. Figure 6 shows a comparison of the experimental centerline velocities and the computed centerline velocities with and without the turbulence relaxation model. The computation without the relaxation model initially ($x/D=0.1$) predicts the velocity field well. The program continues to predict the velocity well through 0.5 diameter downstream. At $x/D=1$, the program begins to underpredict the velocity and this trend

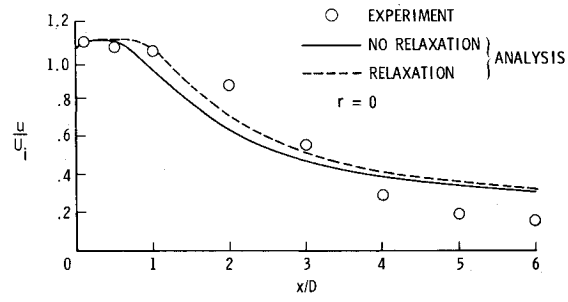

Fig. 6 Comparison of computed and experimental centerline velocities.

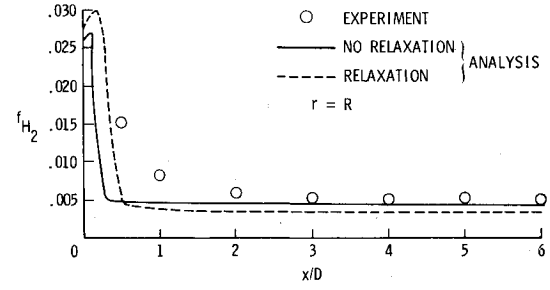

Fig. 7 Axial decay of H_2 mass fraction at outer pipe wall.

continues through $x/D=3$, where the program begins to overpredict the velocity field somewhat. The calculation using the turbulence relaxation model agrees well with the data up to 1 diameter downstream of the step. The code then again underestimates the centerline velocity through $x/D=3$, although the agreement with data is improved as compared to the analysis without relaxation. Beyond 4 diameters, calculations with and without relaxation are nearly the same.

The comparisons discussed above indicate that the predicted growth of the primary air jet and the mixing of the primary jet with the hydrogen behind the step is too rapid between 1 and 3 diameters downstream. Beyond 3 diameters, the code predicts that the mixing is less rapid than the experiment indicates. The prediction with the relaxation model agrees better with the data, since the overall turbulent viscosity level is lower behind the step. This reduced viscosity level is due to a "memory" of lower viscosity levels upstream of the step that are retained by the relaxation model and used in the calculation of the overall viscosity field.

A comparison of measured and computed hydrogen mass fraction along the pipe wall is given in Fig. 7. The program

predicts a more rapid mixing of hydrogen fuel and air than indicated by the experiment. The prediction is improved, however, by the relaxation model, which indicates a slower, although still too rapid, rate of mixing. The code indicates that mixing along the pipe wall is complete after about 1.25 diameters without relaxation and 2 diameters with relaxation, whereas the experiment shows that mixing is complete after about 3 diameters downstream. The experiment and prediction agree reasonably well beyond 3 diameters downstream. These trends are consistent with the streamwise velocity results presented above, indicating that the predicted mixing of hydrogen and air is initially too rapid, and that the predicted mixing rate is improved by introducing into the flow a memory of the lower level of turbulence ahead of the step.

A comparison of the radial distribution of mean axial velocity at seven stations downstream of the step is given in Fig. 8. The agreement between calculation and data is reasonably good between 1 and 4 diameters with the greatest disparity at 2 diameters downstream as can also be seen in Fig. 6. The initial radial mixing at $x/D=0.5$ is again too rapid, and the mixing between $x/D=4$ and 6 is slower than the experiment indicates. These results are again consistent with the axial comparisons given in Figs. 6 and 7.

The predicted region of separated flow can also be compared with the experimental measurement by using Fig. 8. Separated flow behind the step is present in both the experiment and the computation between approximately $x/D=0$ and 3. Nearer the step ($x/D=0.5$), the experimental data indicates a separated region that begins at 0.6 outer pipe radii, R, with a maximum reverse velocity, $u/U_i=-0.1$, whereas the analysis predicts the separation begins at $r/R=0.75$ with a maximum velocity $u/U_i=-0.2$. The agreement improves further downstream at $x/D=1$ and 2 with reattachment indicated in both the experiment and computation at about $x/D=3$.

Comparisons of the computed and experimental radial distribution of hydrogen mass fraction are given in Fig. 9. Only the computational results without turbulence relaxation are given here since they differ little from the results with relaxation. The trends exhibited in earlier comparisons are also present in Fig. 9. The program predicts radial mixing of hydrogen and air that is too rapid near the step ($x/D=0.5$), but agreement between computation and data improves further downstream as the fully mixed value is approached.

The nonreacting comparisons are concluded in Fig. 10, which shows the axial distribution of wall static pressure. The computation indicates a small decrease in wall pressure, followed by an earlier increase in pressure at $x/D=0.5$ as compared to the experiment. The experiment also shows a small decrease in pressure followed by an increase at $x/D=1$. Both

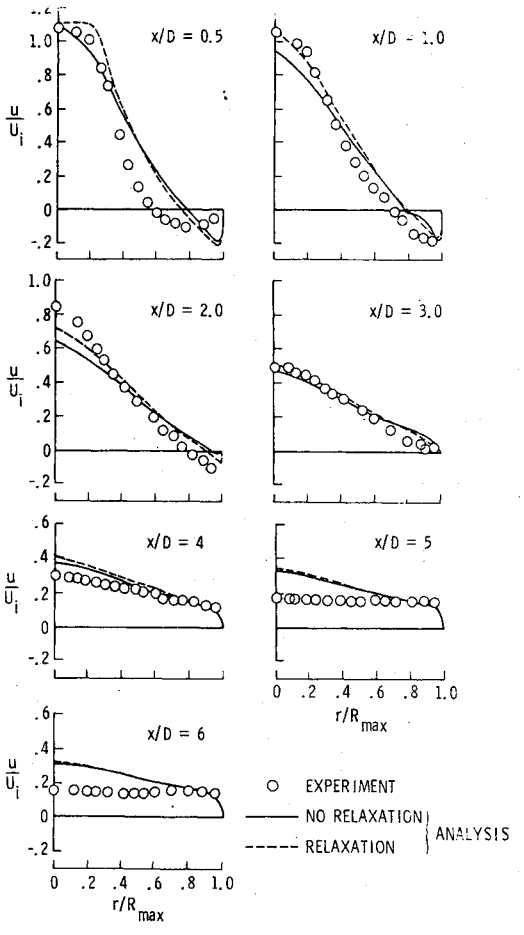

Fig. 8 Radial distribution of mean axial velocity.

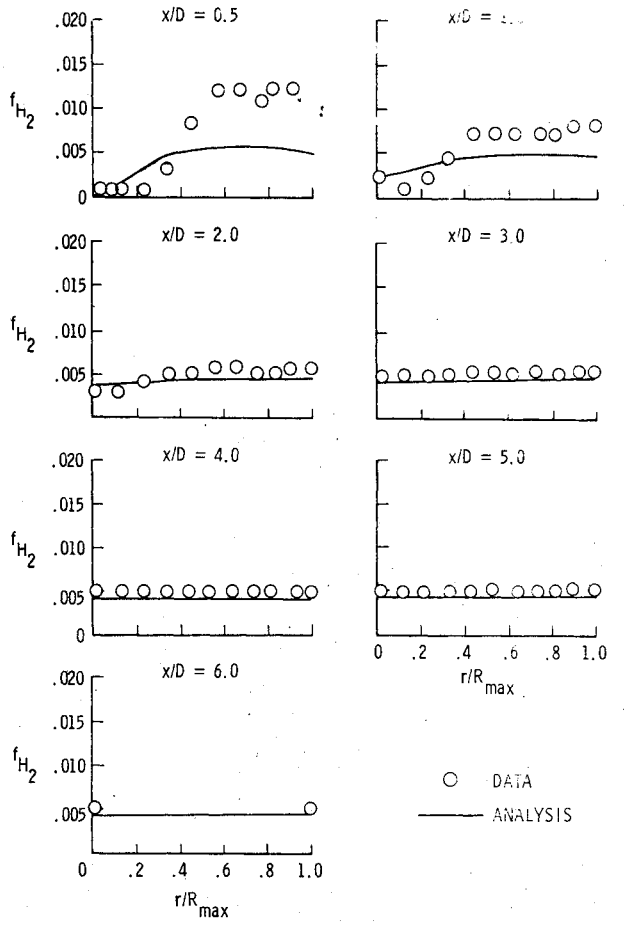

Fig. 9 Radial distribution of hydrogen mass fraction.

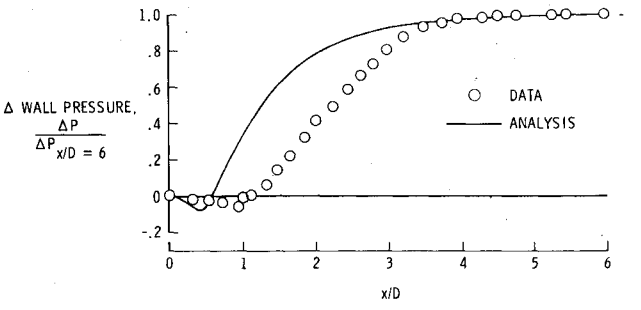

Fig. 10 Axial distribution of wall static pressure.

the analysis and experiment asymptotically approach the exhaust pressure with nearly identical values downstream of $x/D = 3$. The earlier increase in computed wall pressure is also consistent with the prior comparisons and is caused by more rapid mixing of the primary air jet and secondary hydrogen, resulting in the prediction of a fully developed flowfield further upstream, as compared to the experimental results.

The above nonreacting calculations required 150,000 time steps to reach steady-state conditions on the NASA Langley CYBER-203 vector processing computer. The present algorithm, which is fully vectorized for the CYBER-203, exhibits a compute rate of -2.5×10^{-5} s per iteration per grid point. Therefore, the total CPU time required to relax the governing equations to steady state was approximately 4.6 h. It should be noted that no significant changes in the solution were noted after 100,000 time steps, requiring approximately 3 h of CPU time, and the relaxation was continued simply to drive the temporal error terms to lower order and to assure that steady-state conditions had been met.

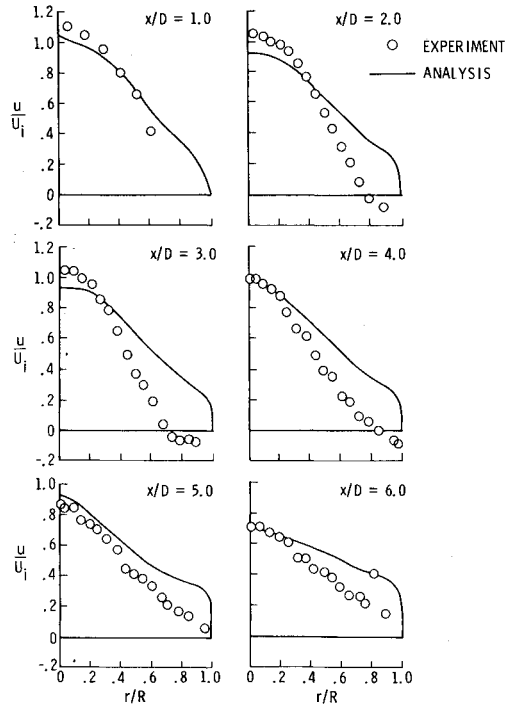

Fig. 11 Radial distribution of mean axial velocity with chemical reaction.

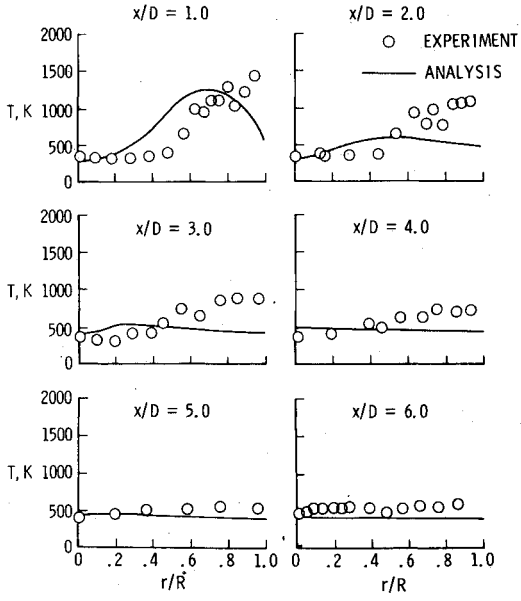

Fig. 12 Radial distribution of mean static temperature.

Comparisons of experimental and analytical results for the dump combustor with a chemically reacting flowfield are given in Figs. 11 and 12. These comparisons are considered preliminary since it is recognized that very good agreement between nonreacting data and computations is required before detailed comparisons with reacting flow can be completed. In addition, both the experimental data and the analysis exhibited a temporal unsteadiness when the flowfield was undergoing chemical reaction. Such an unsteadiness is typical in chemically reacting subsonic flows, and the analysis may be responding to this phenomenon to some extent.

Chemical reaction was introduced into the dump combustor analysis by allowing the nonreacting flow described earlier to react as dictated by the complete reaction chemistry model. The flowfield was relaxed for an additional 50,000 time steps beyond the steady-state nonreacting result, but the temporal error term, $\Delta u/u$, as noted above, could not be reduced below the order of 10^{-3}. Pertinent trends in the reacting flowfield parameters relative to nonreacting results had been established at this time, however, and these results are reported below.

Figure 11 shows the experimental and computed radial distribution of mean axial velocity with the flow undergoing chemical reaction. By comparing Fig. 11 with the nonreacting results given in Fig. 8, it can be seen that chemical reaction has the effect in both the experiment and the analysis of retarding the mixing of the air and hydrogen streams. Whereas the mixing is essentially complete with no reaction at the end of the duct, there is a significant radial gradient of streamwise velocity remaining with chemical reaction indicating that overall mixing of the two streams is not complete.

The experimental and computed radial distributions of static temperature are presented in Fig. 12 for the reacting flowfield. The present data and the analytical results compare fairly well in the latter third of the duct, but the comparison further upstream is not good. The total hydrogen mass fraction (equal to the sum of the mass fraction of hydrogen gas and elemental hydrogen in water) given by the data and the analysis is also in better agreement radially in the latter portion of the duct. Further upstream, the data indicate slower mixing than the analysis with higher experimental concentrations of total hydrogen near the wall. This allows a higher degree of actual chemical reaction near the pipe wall, and, therefore, higher temperatures are measured experimentally relative to the values determined in the computation.

Conclusions

A computer program has been developed to model the turbulent reacting flowfield in an axisymmetric ramjet dump combustor. The program was used to compute the flowfield in a dump combustor simulator from which detailed nonreacting and reacting experimental data had been collected. Comparisons between the nonreacting experimental data and the computation indicate fair agreement overall. Reattachment of the separated flow downstream of the step is predicted well by the program relative to the data, but the experiment indicates that the separated region is transversely thicker and has lower peak reverse velocities. The program also overpredicts the rate of mixing of the air and hydrogen streams. The overprediction is likely due to the algebraic eddy-viscosity turbulence model that is used. This model is empirical and cannot model the very complex turbulence field present in the flow. The nonreacting flow was solved on several coarser finite difference grids without any significant variation in results;

therefore, the solution appears to be relatively grid independent.

The dump combustor flowfield was also computed by the program while the flow was undergoing chemical reaction. Although the results were preliminary in nature, they did indicate consistent trends when compared with the experimental data. Both the data and analysis indicated a significant retardation in mixing of the hydrogen and air when undergoing chemical reaction as compared to the nonreacting flow. Heat release in the confined duct thus lowered the rate of fuel-air mixing.

References

[1]Hutchinson, P., Khalil, E. E., and Whitelaw, J. H., "Measurement and Calculation of Furnace-Flow Properties," *Journal of Energy*, Vol. 1, July-Aug. 1977, pp. 212-219.

[2]Abou Ellail, M.M.M., Gosman, A. D., Lockwood, F. C., and Megahead, T.E.A., "Description and Validation of a Three-Dimensional Procedure for Combustion Chamber Flows," Imperial College, England, Rept. FS/77/27, 1977.

[3]Edelman, R. B., Harsha, P. T., and Schmotolocha, S., "Modeling Techniques for the Analysis of Ramjet Combustion Processes," AIAA Paper 80-1190, June 1980.

[4]Harsha, P. T., Edelman, R. B., Schmotolocha, S. N., and Pederson, R. J., "Combustor Modeling for Ramjet Development Programs," AGARD CP 307, March 1982, pp. 29-1-18.

[5]Viets, H. and Drewry, J. E., "Quantitative Predictions of Dump Combustor Flowfields," *AIAA Journal*, Vol. 19, April 1981, pp. 484-491.

[6]Swithenback, J., Poll, I., Vincent, M. W., and Wright, D. D., "Combustion Design Fundamentals," *Fourteenth Symposium (International) on Combustion*, The Combustion Institute, Pittsburgh, Pa., 1973, pp. 627-636.

[7]Smith, G. D. and Giel, T. V., "An Experimental Investigation of Reactive, Turbulent, Recirculating Jet Mixing," AEDC-TR-79-79, May 1980.

[8]Drummond, J. P., "Numerical Study of a Ramjet Dump Combustor Flow Field," AIAA Paper 83-0421, Jan. 1983.

[9]Smith, R. E. and Weigel, B. L., "Analytic and Approximate Boundary Fitted Coordinate Systems for Fluid Flow Simulation," AIAA Paper 80-0192, Jan. 1980.

[10]Roberts, G. O., "Computational Meshes for Boundary Layer Problems," *Lecture Notes in Physics*, Springer-Verlag, New York, 1971, pp. 171-177.

[11]Thomas, P. D., Vinokur, M., Bastianon, R., and Conti, R. J., "Numerical Solution for the Three-Dimensional Hypersonic Flow Field of a Blunt Delta Body," *AIAA Journal*, Vol. 10, July 1972, pp. 887-894.

[12]Zelazny, S. W., Baker, A. J., and Rushmore, W. L., "Modeling of Three-Dimensional Mixing and Reacting Ducted Flows," NASA CR-2661, April 1976.

[13]Shang, J. S. and Hankey, W. L., "Numerical Solution for Supersonic Turbulent Flow Over a Compression Ramp," *AIAA Journal*, Vol. 13, Oct. 1975, pp. 1368-1374.

[14]Kollman, W., *Prediction Methods for Turbulent Flows*, von Karman Institute for Fluid Dynamics, Hemisphere Publishing Co., New York, 1980, pp. 259-350.

[15]MacCormack, R. W., "The Effect of Viscosity in Hypervelocity Impact Cratering," AIAA Paper 69-354, April 1969.